



Article

# CuFeAl Nanocomposite Catalysts for Coal Combustion in Fluidized Bed

Aleksandr V. Fedorov \*, Nikolay A. Yazykov, Olga A. Bulavchenko, Andrey A. Saraev ,  
Vasily V. Kaichev and Vadim A. Yakovlev

Boreskov Institute of Catalysis, Lavrentev Ave., 5, 630090 Novosibirsk, Russia; yazykov@catalysis.ru (N.A.Y.); isizy@catalysis.ru (O.A.B.); asaraev@catalysis.ru (A.A.S.); vvk@catalysis.ru (V.V.K.); yakovlev@catalysis.ru (V.A.Y.)

\* Correspondence: fedorov@catalysis.ru

Received: 24 April 2020; Accepted: 21 May 2020; Published: 24 May 2020



**Abstract:** A method of oil-drop granulation was suggested for the preparation of spherical CuFeAl nanocomposite catalysts. The catalysts were characterized by a set of physicochemical methods (X-ray diffraction, temperature-programmed reduction by H<sub>2</sub>, low-temperature nitrogen adsorption, crushing strength) and tested in the oxidation of CO and burning of brown coal in a fluidized bed. It was found that the catalysts have high mechanical strength (16.2 MPa), and their catalytic properties in the oxidation of CO are comparable to the characteristics of industrial Cr-containing catalysts. It was shown that the addition of pseudoboehmite at the stage of drop formation contributes to the production of uniform spherical high-strength granules and facilitates the stabilization of the phase state of the active component. The use of CuFeAl nanocomposite catalysts for the burning of brown coal provides a low emission of CO (600 ppm) and NO<sub>x</sub> (220 ppm) and a high degree of coal burnout (95%), which are close to those of the industrial Cr-containing catalysts (emission of CO is 700 ppm, NO<sub>x</sub>—230 ppm, and degree of coal burnout is 95%).

**Keywords:** catalytic combustion; fluidized bed; CO oxidation; oil-drop granulation; iron oxide; copper oxide

## 1. Introduction

The method of burning organic materials in a fluidized catalyst bed has several advantages over traditional methods of combustion [1–5]. In particular, the lower temperature of the process allows one to reduce the requirements for construction materials and to prevent side endothermic reactions leading to the formation of toxic nitrogen oxides (NO<sub>x</sub>). Fluidized bed catalytic combustion provides higher heat densities in the combustion zone due to the localization of oxidation reactions on the catalyst surface, which in turn reduces the size, weight, and capital cost of industrial catalytic installations [6,7].

The catalytic combustion of solid fuels in a fluidized bed imposes a number of requirements for industrial catalysts:

1. High catalytic activity;
2. High mechanical strength and attrition resistance;
3. Spherical shape and narrow distribution of the granule size;
4. Catalytic stability throughout the catalyst lifetime.

The high activity of catalysts is required primarily due to the need to achieve higher levels of fuel combustion efficiency, as well as low levels of harmful gas emissions (CO, CH<sub>4</sub>, and NO<sub>x</sub>). The high mechanical strength is required due to the severe operating conditions in a fluidized bed [8]. The spherical shape of granules helps to reduce the catalyst waste due to attrition. The catalytic stability

requires high sustainability of the catalyst not only to process the conditions (high temperature, redox environment), but also catalytic poisons (sulfur oxides, alkaline metals, etc.) [2,9–11].

The oil-drop granulation method allows the obtaining of spherical  $\text{Al}_2\text{O}_3$  granules, which can be used as a support for the catalysts operating in a fluidized bed [12–14]. The catalysts that satisfy the requirements above and that are commonly used for fluidized bed combustion are Cr-containing catalysts supported on alumina granules [15]. However, a significant drawback of these catalysts is the presence of toxic chromium, which inevitably pollutes the atmosphere as a result of attrition [16]. Iron oxide can be a good alternative to the chromium-containing active component, since catalysts based on  $\text{Fe}_2\text{O}_3$  have a significant activity in deep oxidation [17–19], less toxicity, and a significantly lower cost. Moreover, as we have previously shown, the addition of aluminum and copper oxides can substantially increase the catalytic activity of iron oxide-based catalysts [20–24]. In addition, the introduction of alumina into  $\text{Fe}_2\text{O}_3$  enhances the dispersion of iron oxide particles and, as a result, increases the activity of the catalyst [24]. In turn, the addition of copper lowers the reduction temperature of iron oxide and leads to the formation of copper-containing phases, thereby increasing the activity of the catalyst in the oxidation of CO [22,24]. It was also shown that a nanodispersed CuFeAl catalyst is highly active in the oxidation of CO [20,25]. In the present work, the powder of the CuFeAl catalyst was used as the active component for the preparation of spherical granules of the CuFeAl nanocomposite catalyst.

The spherical granules of the CuFeAl nanocomposite catalyst were prepared by the oil-drop granulation method. The active component was added at the stage of preparing the pseudo-sol, followed by drop formation of the resulting suspension. The proposed approach can significantly increase the content of the active component and, as a result, the activity of a synthesized catalyst. This paper presents the results of a study of the physicochemical and catalytic properties of the CuFeAl nanocomposite catalyst. The catalyst was tested in the burning of brown coal in a fluidized bed in comparison with a common chromium-containing industrial catalyst.

## 2. Materials and Methods

### 2.1. Catalyst Preparation

The powdered CuFeAl catalysts were prepared by the melting of copper, iron, and aluminum nitrates  $\text{Cu}(\text{NO}_3)_2 \cdot 3\text{H}_2\text{O}$  (98.0%, ReaHim Ltd., Moscow, Russia),  $\text{Fe}(\text{NO}_3)_3 \cdot 9\text{H}_2\text{O}$  (99.0%, ReaHim Ltd., Moscow, Russia), and  $\text{Al}(\text{NO}_3)_3 \cdot 9\text{H}_2\text{O}$  (99.0%, ReaHim Ltd., Moscow, Russia). To prepare 10 g of the CuFeAl nanocomposite catalyst, the nitrates (1.55 g of  $\text{Cu}(\text{NO}_3)_2 \cdot 3\text{H}_2\text{O}$ , 39.82 g of  $\text{Fe}(\text{NO}_3)_3 \cdot 9\text{H}_2\text{O}$ , 12.70 g of  $\text{Al}(\text{NO}_3)_3 \cdot 9\text{H}_2\text{O}$ ) were mixed; the mixture was heated to give a homogeneous melt of hydrate salts ( $\approx 130$  °C) and then was kept at a temperature of 200 °C, forming a solid precipitate. Finally, the resulting dry powder was calcined at 450 °C for 1 h in air using a furnace (WiseTherm FX-03, Daihan Scientific Co. Ltd., Seoul, South Korea). The powdered catalysts consisted of oxides of the following calculating composition: 5.0 wt% CuO, 77.9 wt%  $\text{Fe}_2\text{O}_3$ , and 17.1 wt%  $\text{Al}_2\text{O}_3$ .

The spherical CuFeAl nanocomposite catalysts were prepared by the oil-drop granulation method. For this, 2M  $\text{HNO}_3$  was added dropwise under stirring for 10 min using a mechanical stirrer (2000 rpm, Eurostar digital, IKA-Werke GmbH, Staufen im Breisgau, Germany) to the suspension of aluminum hydroxide  $\text{AlOOH}$  (76.0 wt%  $\text{Al}_2\text{O}_3$ , <0.002 wt%  $\text{Na}_2\text{O}$ , Pural SCF, Sasol Germany GmbH, Hamburg, Germany) in distilled water. The obtained suspension was diluted with distilled water and then was settled. A portion of the CuFeAl catalyst was added to the resulting suspension, and the obtained slurry was thoroughly mixed using the mechanical stirrer (2000 rpm, 10 min). Formation of spherical granules was carried out by generating sol droplets (3 mm diameter) with an adjutage, passing-through a paraffin oil layer, followed by gelating and aging in an ammonia layer. Resultant granules were slowly dried in an argon environment for 10 h at room temperature followed by 1 h at 100 °C and then calcined in air at 400 °C for 1 h and at 700 °C for 1 h with a heating rate of 15 °C/min. The sample was cooled to room temperature in a calcining furnace (5–10 °C/min). Figure 1 shows a scheme of the

preparation of the spherical CuFeAl nanocomposite catalysts. Table 1 shows the conditions used for the preparation of the catalysts by drop granulation.

**Table 1.** Conditions used for preparation of the spherical CuFeAl composite catalysts. The data for obtaining 10 g of spherical catalyst.

AIOOH Content, wt%	HNO <sub>3</sub> :Al <sub>2</sub> O <sub>3</sub> Molar Ratio	H <sub>2</sub> O Content, wt%	Powdered Catalyst, Weight, g	AIOOH Weight, g	2 M HNO <sub>3</sub> , Vol. mL	H <sub>2</sub> O Weight, g
20	0.100	85	8.40	2.10	1.47	56.6
30	0.084	82	7.59	3.24	1.90	45.6
40	0.067	78	6.71	4.47	2.10	35.5
50	0.050	75	5.69	5.69	1.99	30.0

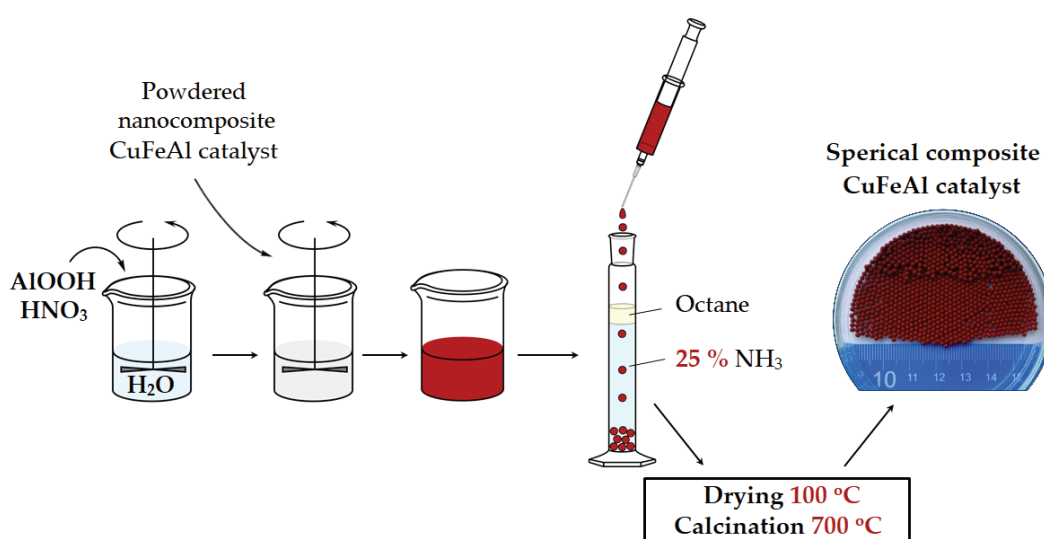


**Figure 1.** Scheme of the spherical CuFeAl nanocomposite catalyst preparation.

To prepare a 2M HNO<sub>3</sub> solution, we used 70% nitric acid (ReaHim Ltd., Russia) and 25% ammonia solution (ReaHim Ltd., Russia). As the paraffin oil layer, n-octane CH<sub>3</sub>(CH<sub>2</sub>)<sub>6</sub>CH<sub>3</sub> (95.0%, “ReaHim” Ltd., Moscow, Russia) was used.

## 2.2. X-ray Diffraction

The phase composition of the CuFeAl nanocomposite catalysts was studied by X-ray diffraction using a D8 Advance X-ray diffractometer (Bruker, Ettlingen, Germany) equipped with a Lynxeye linear detector. The monochromatic Cu K $\alpha$  radiation ( $\lambda = 1.5418 \text{ \AA}$ ) was applied for analysis. The XRD patterns were obtained in the  $2\theta$  range from  $15^\circ$  to  $80^\circ$  with a step of  $0.05^\circ$ . The coherent scattering region (average crystallite size) was determined using the Scherrer equation from the full width half maximum of the diffraction peaks. The coherent scattering region of hematite was calculated from the 140 reflection.

## 2.3. Specific Surface Area Analysis

The catalysts were analyzed by low-temperature nitrogen porosimetry using an automated volumetric adsorption analyzer ASAP 2400 (Micromeritics Instrument Corp., Norcross, GA, USA). Before the recording of the nitrogen adsorption isotherms, the samples were outgassed at  $150^\circ\text{C}$  and a pressure of 0.13 Pa for 4 h. The initial branch of the N<sub>2</sub> adsorption isotherm in a range of  $P/P_0$  from 0.05 to 0.2 was used to calculate the specific surface area (SSA) by the Brunauer–Emmett–Teller method.

#### 2.4. Crushing Strength

The crushing strength of the spherical alumina granules was measured using a commercial strength tester (MP-9S, Novosibirsk Instrument-Building Plant, Novosibirsk, Russia). The spheres were loaded diametrically and then pressed between two rigid platens at a constant crosshead speed of 0.1 mm/s. The load at which the fracture of the sphere occurred was recorded as the crushing strength ( $F$ ). The fracture stress ( $\sigma$ ) was used to describe the mechanical strength of porous materials. It is known that  $\sigma$  does not depend on the shape and size (tablets, spheres, etc.) of pellets in contrast to the crushing strength. For spherical pellets, Hiramatsu and Oka showed [26] that the fracture stress is estimated from the crushing strength as follows:

$$\sigma = \frac{2.8F}{\pi d^2},$$

where  $d$  is the granule diameter, and  $F$  is the crushing strength. The number of measurements was 100 granules.

#### 2.5. Temperature-Programmed Reduction

The temperature-programmed reduction of TPR-H<sub>2</sub> was performed using a Chemosorb analyzer (Modern Laboratory Equipment, Novosibirsk, Russia). For all experiments, a sample (0.1 g) was first placed in a U-tube quartz reactor. The sample was then heated up to 900 °C with a constant heating rate of 8 °C/min using a 10% H<sub>2</sub>/Ar flow (30 mL/min) as a reducing agent. The hydrogen consumption was measured with a thermal conductivity detector.

#### 2.6. Catalytic Activity Tests

The catalytic tests were performed using a catalytic setup with a flow-fixed bed reactor. A powdered sample with a particle size of 0.2–0.5 mm was loosely packed into a tubular U-shaped quartz reactor with a 3.8-mm inner diameter and a 10-mm length. The catalyst volume was 113 mm<sup>3</sup>. During the experiments, a gas mixture containing 20 vol.% O<sub>2</sub> and 80 vol.% He was passed through the reactor with a constant flow rate of 30 cm<sup>3</sup>/min and CO was injected into the gas mixture in the pulse mode (0.1 cm<sup>3</sup> pulse<sup>-1</sup> for 0.75 s). The catalyst was heated from 25 to 350 °C with a constant rate (30 °C/min). Simultaneously, the concentrations of CO were monitored at the reactor outlet with a thermal conductivity detector and the catalytic activity was determined as the temperature of the 50%-CO conversion ( $T_{50}$ ). The catalytic activity of synthesized catalysts was compared with a widely used commercial catalyst—Cu<sub>x</sub>Mg<sub>1-x</sub>Cr<sub>2</sub>O<sub>4</sub>/Al<sub>2</sub>O<sub>3</sub> (ForAlumina Ltd., Yarovoye, Russia). The commercial catalyst is the mix of copper oxide and magnesium chromites deposited on spherical alumina granules. Composition: 1.7% of CuO, 3.6% of MgO, 17.0% of Cr<sub>2</sub>O<sub>3</sub>, and the rest of Al<sub>2</sub>O<sub>3</sub>. The specific surface area for the commercial catalyst is 120 m<sup>2</sup>/g.

#### 2.7. Coal Combustion in a Fluidized Bed of a Catalyst

A scheme of an installation for coal combustion is shown in Figure 2. The installation consists of a fluidized bed reactor with a diameter of 40 mm, of a coal bunker with a screw feeder and an ejector to transfer fuel into the reactor, and of an analysis system.

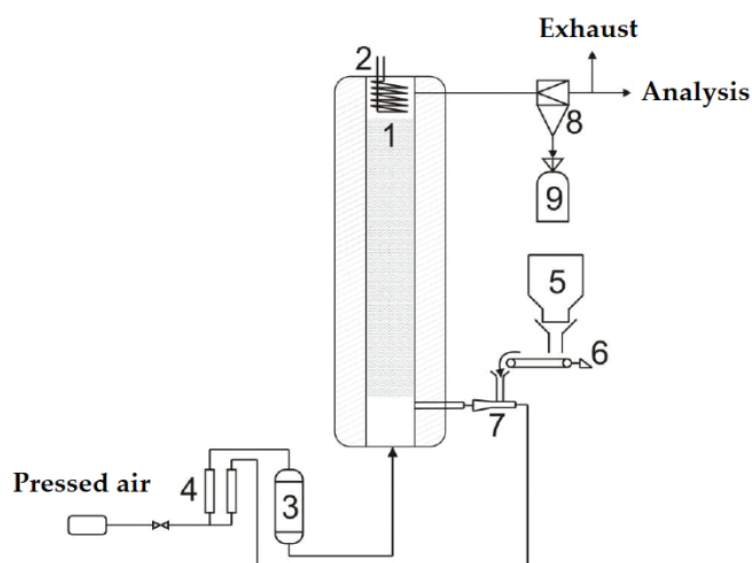


**Figure 2.** Scheme of the installation for coal combustion in the fluidized bed of a catalyst: 1—reactor; 2—heat exchanger; 3—air heater; 4—rotameters; 5—coal bunker; 6—screw feeder; 7—ejector; 8—cyclone; 9—ash collection bunker.

The preheated air was fed to the reactor bottom to start up the reactor. Airflow rates were controlled with rotameters. Ash particles after the reactor were separated from flue gases in the cyclone and passed into the ash collection bunker. The brown coal combustion was carried out in the fluidized bed of the catalyst with a granule diameter of 1.4–2.0 mm. The loading of the catalyst was 500 mL. The coal combustion was carried out at a constant temperature of 700 °C, an airflow rate of 2.76 m<sup>3</sup>/h, and a coal consumption of 290 g/h (air excess of 3.1). The concentration of pollutants (NO, NO<sub>2</sub>, and CO) in flue gases was determined with a Polar analyzer (Promecopribor Ltd., Moscow, Russia). The degree of burning solid fuel ( $\beta$ ) was determined by

$$\beta = \frac{10000(A - A_0)}{A(100 - A_0)},$$

where  $A$  is the ash content of dry coal and ash content of remainder after combustion, in percentage. Characteristics of coal are presented in Table 2. The total moisture content of the fuels was determined in accordance with ISO 5068-1:2007. The volatile matter yield was determined in accordance with ISO 5071-1:2013. The ash content in brown coal and product residues was determined in accordance with GOST (State Standard) 55661–2013. The elemental composition of brown coal was determined using a CHNS VARIO EL CUBE elemental analyzer (Elementar Analysensysteme GmbH, Langenselbold, Germany).

**Table 2.** Physicochemical characteristics of brown coal.

Moisture, %	Ash Content, %	Volatiles, %	C, %	H, %	N, %	O, %	S, %
9.8	11.1	48.0	54.6	4.4	1.5	26.9	1.5

### 3. Results and Discussion

#### 3.1. Strength and Activity of Spherical CuFeAl-Composite Catalysts

High mechanical strength and attrition resistance are important characteristics of fluidized bed catalysts. To assess the mechanical strength, the method of measuring the crushing strength of individual granules is usually used as an express method [27]. For the catalysts used in fluidized bed

combustion, the minimum fracture stress should be more than 7 MPa [8]. The mechanical interaction of the catalyst granules with such a fracture stress leads mainly to their attrition as a result of mutual friction, and the catalyst loss in this case usually does not exceed 0.5% per day. In contrast, the lower values of fracture stress (<7 MPa) lead to the significant cracking of the catalyst granules during operation, and this leads to an increase in catalyst waste, sometimes by more than 5% per day [2]. One of the main objectives of this work was to study the dependence of the fracture stress and activity of a spherical composite CuFeAl catalyst on the content of pseudoboehmite added at the molding stage (Figure 3). It is important to note that at the pseudoboehmite content of less than 20%, it was not possible to obtain uniform spherical granules of the CuFeAl nanocomposite catalyst.

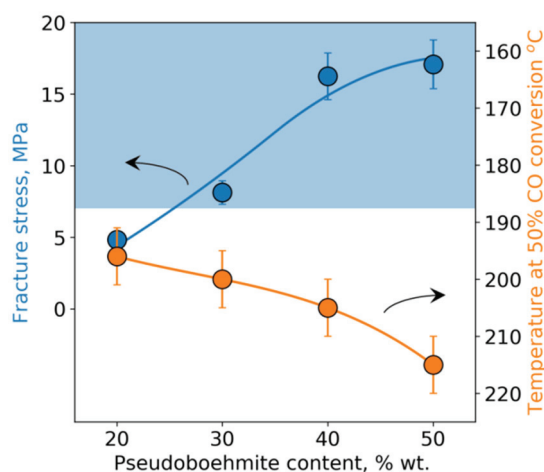


**Figure 3.** Dependence of the strength (the blue curve and circles) and activity (the orange curve and circles) of the CuFeAl nanocomposite catalyst on the pseudoboehmite content. The blue area is a zone of the required strength.

As seen from Figure 3, an increase in the pseudoboehmite content leads to an increase in the strength of the obtained catalyst granules and to a simultaneous decrease in the activity of the catalyst. The monotonic decrease in activity is associated with a decrease in the content of the active component in the catalyst due to its dilution with alumina, which is known to be inactive in deep oxidation reactions. It is worth mentioning that the activity of all four catalysts with the different pseudoboehmite content exceeds the activity of an industrial catalyst  $\text{Cu}_x\text{Mg}_{1-x}\text{Cr}_2\text{O}_4/\text{Al}_2\text{O}_3$  (composition: 1.7% CuO, 3.6% MgO, 17.0%  $\text{Cr}_2\text{O}_3$ , and the rest  $\text{Al}_2\text{O}_3$ ), for which the temperature of the 50%-conversion of CO is 240 °C.

At a pseudoboehmite content of  $\geq 40\%$ , the obtained granules of the spherical CuFeAl nanocomposite catalyst have a high mechanical fracture stress, exceeding an average of 15 MPa. However, it is necessary to take into account the variance of this value [28–30]. This is important because porous materials contain defects that are randomly distributed over the volume. When a static force is applied, a granule cracks in the place with the maximum concentration of these defects. The presence of these defects and their random distribution lead to a wide distribution of the values of mechanical strength. The Weibull distribution is commonly used for describing the obtained experimental data [28]. However, in our previous work [31], it was shown that for a statistical description of the mechanical strength of alumina-based materials, it is necessary to use a two-parameter Gamma distribution. Note that the parameter  $\alpha$  of Gamma distribution determines the distribution width, and the higher  $\alpha$  is, the narrower the distribution is. The parameters of the Gamma and Weibull distributions were calculated (Table 3) for the obtained CuFeAl nanocomposite catalysts and the industrial Cr-containing catalyst. As seen from the presented data, both the parameter  $\alpha$  and the Weibull modulus  $m$  monotonously decrease with an increase in the pseudoboehmite content, which is accompanied by an increase in the granule strength. The parameter  $\alpha$  for the Cr-containing

catalyst is slightly lower than that for the CuFeAl nanocomposite catalysts. The values of the Weibull modulus  $m$  for the studied catalysts are in the range of 3.5–4.4, which is consistent with the published data. Antonyuk et al. [32] obtained the Weibull modulus  $m \approx 5$  for spherical  $\gamma$ -Al<sub>2</sub>O<sub>3</sub> granules. For a series of water gas shift catalysts based on alumina, M. Zakeri et al. [29] observed values of  $m$  in the range of 2.5–11.

**Table 3.** Catalytic and mechanical properties of the CuFeAl composite and Cr-containing catalysts.

Catalyst	Pseudoboehmite Content, wt%	T <sub>50</sub> , °C	Fracture Stress, MPa	Fraction of Fragile Granules (<7 MPa), %	$\alpha$ Parameter	$m$ , Weibull Modulus
CuFeAl nanocomposite catalysts	20	196	4.3	94	13.4	4.4
	30	200	8.1	35	12.8	4.1
	40	205	16.2	0.7	12.2	3.9
	50	215	17.1	0.6	11.2	3.5
Cu <sub>x</sub> Mg <sub>1-x</sub> Cr <sub>2</sub> O <sub>4</sub> /Al <sub>2</sub> O <sub>3</sub>	-	240	14.4	2.7	10.0	3.5

Based on the obtained Gamma distribution parameters, the fraction of granules with the fracture stress less than 7 MPa was estimated (Table 3). The calculation procedure is described elsewhere [31]. When the pseudoboehmite content achieves 40–50%, the fraction of granules with the low fracture stress decreases to less than 1% (0.6–0.7%). At the same time, in the case of the industrial Cr-containing catalyst, the fraction of fragile granules is about 2.7%. This is due to both the lower strength of the industrial catalyst granules and a lower Gamma distribution parameter  $\alpha$ . Consequently, it can be expected that the loss of the CuFeAl nanocomposite catalyst during operation in the fluidized bed will be lower than that of the Cr-containing industrial catalyst.

According to the data obtained, it can be concluded that the developed spherical CuFeAl nanocomposite catalyst has high mechanical strength and activity in the oxidation of CO, which are comparable to the characteristics of the industrial Cr-containing catalyst. The catalyst with the 40% pseudoboehmite content was used for further research.

### 3.2. Thermal Stability of Spherical CuFeAl Nanocomposite Catalysts

As noted above, one of the important requirements for catalysts of deep oxidation in a fluidized bed is their thermal stability [33–35]. This requirement arises from the high operating temperature of about 700–750 °C and short-term and/or local overheating up to 1000 °C [2]. Therefore, one of the main goals of this study was to investigate the effect of temperature treatment at 800 °C on the activity and physicochemical properties of the spherical CuFeAl nanocomposite catalyst. Figure 4 shows the dependence of activity and specific surface area of the studied catalysts on the calcination time at a temperature of 800 °C.

As seen from Figure 4, the activity of the spherical CuFeAl nanocomposite catalyst decreases during the first 5 h of calcination and stabilizes after that. Figure 4 also shows that the decrease in surface area is slower than the decrease in activity. It can be assumed that the initial decrease in activity is associated with the sintering of the active component and the excipient (alumina introduced at the oil-drop granulation stage), since the spherical CuFeAl catalyst is a complex composite consisting of the active component and the excipient. A further decrease in the surface is accompanied by the sintering of alumina (excipient), which is not active in deep oxidation reactions. After 5 h, there is no noticeable decrease in activity and specific surface area due to stabilization of the catalyst structure. In addition, the activity of the spherical catalyst calcined at 800 °C is higher than that of the industrial Cr-containing catalyst over the whole range of calcination times (Figure 4).

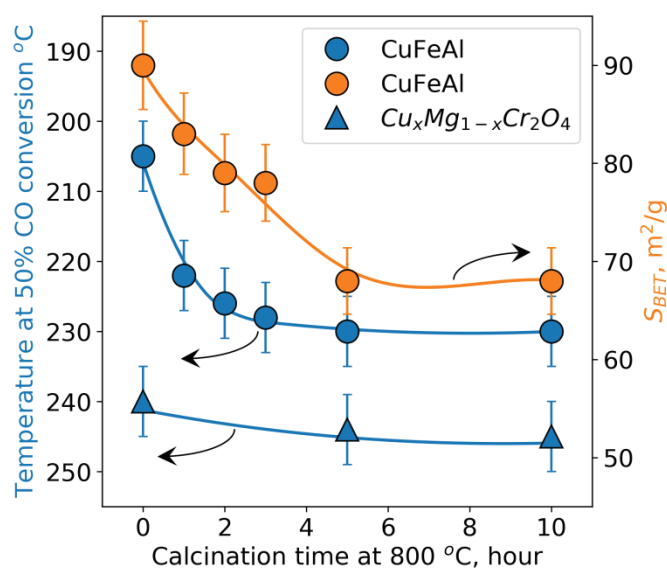


**Figure 4.** Dependence of activity (the blue curves and circles) and specific surface area (the orange curve and circles) of the studied catalysts on the calcination time at 800 °C, and dependence of activity (the blue curves and triangles) of the commercial catalysts.

In the case of the initial powdered catalyst, its activity and specific surface area decrease stronger than those of the spherical catalyst. Table 4 demonstrates the effect of heat treatment on the powdered and spherical catalysts. As seen, the temperature of 50%-conversion of CO for the powdered catalyst increases from 190 to 240 °C (50 °C), while for the spherical catalyst, it increases from 195 to 230 °C (35 °C). One can see that in the case of the spherical catalyst, the decrease in catalytic activity is lower than for the powdered catalyst during the calcination at 800 °C for 5 h (Table 4). Since the spherical catalyst consists of a powdered catalyst and alumina introduced at the oil-drop granulation stage, it could be assumed that alumina stabilizes the active component at high temperatures.

**Table 4.** Catalytic and physico-chemical properties of CuFeAl catalysts calcined at different conditions.

Catalyst	Powdered CuFeAl Catalyst		Spherical CuFeAl Catalyst	
	700 °C 1 h	800 °C 5 h	700 °C 1 h	800 °C 5 h
T <sub>50%</sub> , °C	190	240	195	230
SSA, m <sup>2</sup> /g	60	12	90	68
Composition, wt%	CuO	5.0	3.3	
	Fe <sub>2</sub> O <sub>3</sub>	77.9	51.1	
	Al <sub>2</sub> O <sub>3</sub>	17.1	45.6	

Figure 5 shows X-ray diffraction (XRD) patterns of the powdered and spherical CuFeAl nanocomposite catalysts calcined at 700 or 800 °C. As seen, the XRD patterns of all samples contain Fe<sub>2</sub>O<sub>3</sub> hematite reflexes [JCPDS 330664]. The XRD patterns of the spherical catalysts exhibit broad peaks in the 2θ ranges of 45°–48° and 60°–70°. This indicates the presence of γ-Al<sub>2</sub>O<sub>3</sub> [JCPDS 10-0425] formed from pseudoboehmite during calcination. There are no significant differences in the XRD patterns of the spherical catalysts except for an increase in the coherent scattering region (CSR) for hematite, calculated from the 140 reflection (from 58 to 71 nm) for the sample calcined at 800 °C. In contrast, the XRD patterns of the powdered catalysts differ. In the pattern of the sample calcined at 800 °C, there are low-intensity reflections, indicating the formation of spinel (Cu,Al,Fe)<sub>3</sub>O<sub>4</sub> with the

space group  $Fd\bar{3}m$ . In our previous paper [36], it was shown that for the active component with a higher copper content (10 wt% CuO), copper exists mainly in the form of spinel ( $\text{Cu}_{0.24}\text{Fe}_{0.68}\text{Al}_{0.08}$ ) $_3\text{O}_4$  based on iron oxide. This explains its lower activity in comparison with samples containing 5 wt. % CuO, in which copper is in a highly disperse state. Meng-Fei Luo et al. [37] observed the formation of  $\text{CuAl}_2\text{O}_4$  spinel for a catalyst  $\text{CuO}/\text{Al}_2\text{O}_3$  obtained by impregnation and calcination at temperatures above 700 °C. The lower CuO content, as well as the lower calcination temperature, lead to the predominant formation of finely disperse copper-containing particles, which determine the higher activity of these catalysts. Thus, the formation of spinel in the active component calcined at 800 °C may cause a decrease in the activity of these catalysts in the oxidation of CO, along with a decrease in the total specific surface.

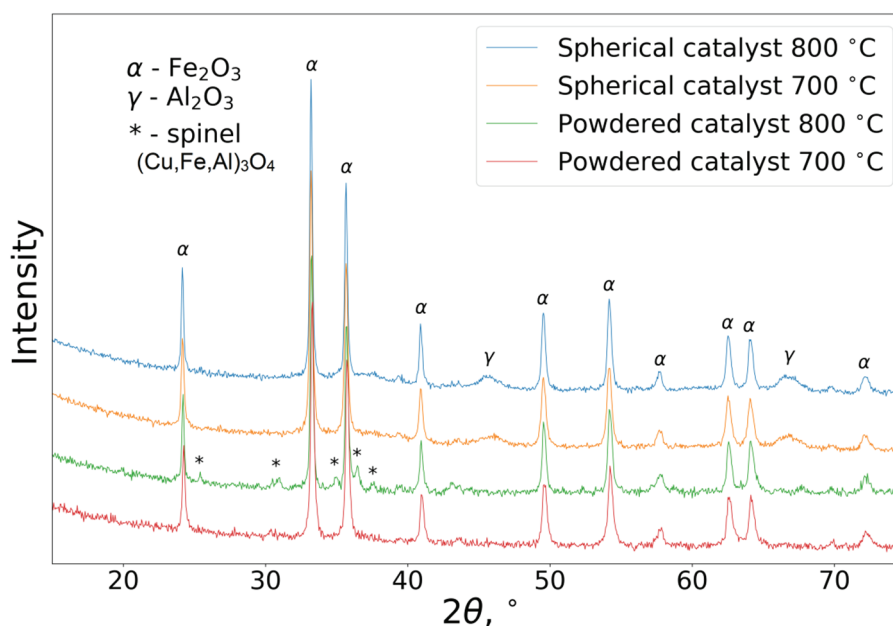
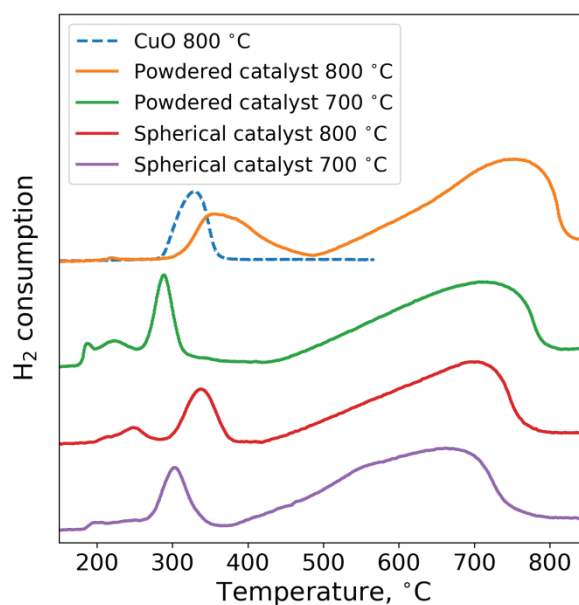


Figure 5. XRD patterns of CuFeAl catalysts.

Figure 6 presents the temperature-programmed hydrogen reduction (TPR- $\text{H}_2$ ) curves for the studied catalysts. Curve profiles consist of several peaks. The first peak at temperatures of 200–250 °C is associated with the reduction of copper oxide to the metallic state:  $\text{CuO} \rightarrow \text{Cu}$  [22,23,37,38]. The peak at 300–350 °C shows the partial reduction of iron(III) oxide:  $\text{Fe}_2\text{O}_3 \rightarrow \text{Fe}_3\text{O}_4$  [22]. The next wide peak at temperatures of 400–900 °C is associated with a step reduction of iron(II,III) oxide to the metallic state:  $\text{Fe}_3\text{O}_4 \rightarrow \text{FeO} \rightarrow \text{Fe}$  [39]. Note that the increase in calcination temperature does not lead to any significant change in the TPR- $\text{H}_2$  profile of the spherical catalyst. The only difference is that the reduction peaks of iron oxides shift toward higher temperatures, which is associated with the agglomeration of  $\text{Fe}_2\text{O}_3$  due to calcination. A similar shift was observed by H. Wang [40] during the calcination of  $\text{CuO}-\text{Fe}_2\text{O}_3$  catalysts for the  $\text{NH}_3$ -SCO reaction. On the contrary, the TPR- $\text{H}_2$  curve of the powder catalyst changes significantly. For the sample calcined at 800 °C, the low-temperature peak of hydrogen absorption disappears. Moreover, the temperature at which the reduction of this sample starts is higher than that of individual copper oxide calcined under the same conditions. This may be caused by copper being in the form of spinel, which is reduced at a higher temperature and which is less active in the oxidation of CO. The formation of spinel in  $\text{CuO}-\text{Al}_2\text{O}_3$  catalysts calcined at temperatures above 700 °C and similar changes in the TPR- $\text{H}_2$  profiles were reported elsewhere [37,38].



**Figure 6.** TPR-H<sub>2</sub> profiles of CuFeAl nanocomposite catalysts.

Based on these results, it can be concluded that the developed spherical CuFeAl composite catalyst has high thermal stability. Moreover, the addition of pseudoboehmite at the stage of drop formation not only contributes to obtaining the uniform high-strength spherical catalyst, but also facilitates stabilization of the phase state of the active component. Heat treatment at 800 °C does not lead to the formation of copper-containing phases with the spinel structure, which are less active in the oxidation of CO. Therefore, the detected decrease in activity is mainly caused by a decrease in the total specific surface area as a result of the sintering of the active component.

### 3.3. Coal Combustion in a Fluidized Bed of a Catalyst

The final stage of this work included the production of a batch of the catalyst and its testing in the process of burning brown coal in a fluidized bed. The combustion was carried out for 2 h. The concentration of harmful substances (CO, NO<sub>x</sub>, and CH<sub>4</sub>) in the exhaust gases was measured on-line using a gas analyzer with an analysis frequency of 1 Hz. Every 30 min, an ash sample was taken to determine the degree of burnout. Table 5 presents the tests results using three samples: the developed CuFeAl nanocomposite catalyst, the industrial Cr-containing catalyst, and an inert material (quartz sand). The specific surface area for the quartz sand is less than 1 m<sup>2</sup>/g.

**Table 5.** Catalytic properties of the CuFeAl composite and Cr-containing catalysts.

Catalyst	CO, ppm	NO, ppm	Coal Burnout, %
SiO <sub>2</sub> (quartz sand)	>8000	100	70
Spherical CuFeAl nanocomposite catalyst *	600	220	95
Cu <sub>x</sub> Mg <sub>1-x</sub> Cr <sub>2</sub> O <sub>4</sub> /Al <sub>2</sub> O <sub>3</sub>	700	230	95

\* the catalyst was calcined at 700 °C for 1 h.

For both catalysts, the concentrations of harmful substances and the degree of burnout during the experiment were constant (<5% relative difference). First, it is worth noting that with the use of the catalysts, the degree of burnout achieved 95% (in contrast, only 70% for quartz sand). This is determined by the processes of gasification of solid fuel in a fluidized bed of the catalyst. It is known

that coke gasification, as the limiting stage of the combustion process, proceeds on the surface of coal particles along the following main routes:

1.  $C + O_2 \rightarrow CO_2$ ;
2.  $2C + O_2 \rightarrow 2CO$ ;
3.  $C + CO_2 \rightarrow 2CO$ ;
4.  $C + H_2O \rightarrow CO + H_2$ .

At low combustion temperatures, the coke gasification is limited by the diffusion of oxygen to the surface of coke particles with the formation of CO and CO<sub>2</sub> [41]. In the case of catalytic deep oxidation, the concentration of CO in the surface layer of the coke particle, and in the gas phase as a whole, is significantly reduced since the catalyst accelerates the oxidation of CO and volatile organic substances (VOC) to the products of complete oxidation (CO<sub>2</sub> and H<sub>2</sub>O). This significantly increases the diffusion of oxygen to the surface of coke particles and, as a consequence, increases the rate of coke gasification. The combustion in the catalyst bed is schematically shown in Figure 7. It explains the observed increase in the degree of burnout from 70% to 95% and a significant reduction in CO emissions when using the catalysts instead of quartz sand. Moreover, for both the industrial Cr-containing catalyst and the CuFeAl nanocomposite catalyst, the CO emissions are approximately the same and are in the range of 600–700 ppm. The concentration of CH<sub>4</sub> during the combustion for all samples was below the detection limit of the analyzer (<0.01%).

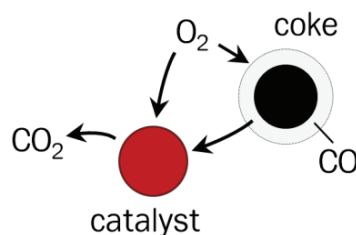


Figure 7. Scheme of coke gasification in a fluidized catalyst bed.

Nitrogen oxides NO<sub>x</sub> (NO and NO<sub>2</sub>) are well known to be among the most common harmful emissions generated during fuel combustion. NO<sub>x</sub> can be formed both as a result of the oxidation of atmospheric nitrogen by a radical mechanism (thermal NO<sub>x</sub>) and as a result of the oxidation of organic fuel compounds containing nitrogen (fuel NO<sub>x</sub>). The contribution of the radical oxidation mechanism at temperatures below 750 °C is insignificant, and NO<sub>x</sub> is mainly formed as a result of the oxidation of nitrogen-containing fuel components [42]. During the catalytic combustion of brown coal in a fluidized bed, the concentration of NO was near 230–240 ppm. The concentration of NO<sub>2</sub> for all samples was <10 ppm, which is determined by the thermodynamic equilibrium of the formation of nitrogen oxides ( $2NO + O_2 \rightleftharpoons 2NO_2$ ) during fuel combustion [43]. In the case of quartz sand, the NO concentration was half of the value observed for the catalysts (~100 ppm). A lower emission of NO in this case was due to a high concentration of CO and, as a consequence, due to a high contribution from the reactions of the reduction of nitrogen oxides [44]:

5.  $NO_2 + CO \rightarrow NO + CO_2$ ;
6.  $NO + 2CO \rightarrow N_2 + 2CO_2$ .

Thus, the use of the CuFeAl nanocomposite catalyst for the burning of brown coal allows one to achieve low concentrations of CO and NO<sub>x</sub> and a high degree of fuel burnout, which is close to that for the industrial Cr-containing catalyst. On the basis of the physico-chemical and catalytic characteristics, it can be concluded that the developed spherical CuFeAl nanocomposite catalyst satisfies the basic requirements for deep oxidation catalysts for a fluidized bed and can be recommended for the combustion of gaseous, liquid, and solid fuels.

#### 4. Conclusions

A series of spherical CuFeAl nanocomposite catalysts was prepared by the oil-drop granulation method. The samples were investigated by XRD, TPR-H<sub>2</sub>, low-temperature nitrogen adsorption, and crushing strength. Their catalytic properties were studied in the oxidation of CO and burning of brown coal. The burning of coal was studied in a fluidized bed of quartz sand, the spherical CuFeAl nanocomposite, and the industrial Cr-containing catalyst. It was shown that the developed spherical CuFeAl nanocomposite catalyst demonstrates high activity in the CO oxidation, slightly exceeding the characteristics of the industrial Cr-containing catalyst. In addition, the mechanical strength characteristics of the synthesized catalyst (fracture stress of about 16 MPa) comply with the requirements for deep oxidation catalysts for a fluidized bed. The developed catalyst has high thermal stability (up to 800 °C). The addition of pseudoboehmite at the stage of drop formation not only leads to the formation of uniform high-strength granules, but also allows one to stabilize the phase state of the active component. Heat treatment at 800 °C does not lead to the formation of a copper-containing phase with the spinel structure, which is less active in the oxidation of CO. The decrease in activity detected during the first few hours of the reaction is mainly caused by a decrease in the total specific surface area as a result of the sintering of the active component. The use of the CuFeAl nanocomposite catalyst for the burning of brown coal provides low concentrations of CO (600 ppm) and NO<sub>x</sub> (220 ppm) as well as a high degree of burnout (95%), which is close to that of the industrial Cr-containing catalyst.

**Author Contributions:** Conceptualization, V.A.Y.; Formal analysis, A.V.F.; Investigation, A.V.F., N.A.Y., O.A.B. and A.A.S.; Visualization, A.V.F.; Writing—original draft, A.V.F.; Writing—review and editing, V.V.K. All authors have read and agreed to the published version of the manuscript.

**Funding:** This work was supported by the Russian Science Foundation, grant 17-73-20157.

**Conflicts of Interest:** The authors declare no conflict of interest.

#### References

1. Ismagilov, Z.R.; Kerzhentsev, M.A. Fluidized bed catalytic combustion. *Catal. Today* **1999**, *47*, 339–346. [[CrossRef](#)]
2. Parmon, V.N.; Simonov, A.D.; Sadykov, V.A.; Tikhov, S.F. Catalytic combustion: Achievements and problems. *Combust. Explos. Shock Waves* **2015**, *51*, 143–150. [[CrossRef](#)]
3. Yazykov, N.A.; Dubinin, Y.V.; Simonov, A.D.; Reshetnikov, S.I.; Yakovlev, V.A. Features of sulfur oils catalytic combustion in fluidized bed. *Chem. Eng. J.* **2016**, *283*, 649–655. [[CrossRef](#)]
4. Iamarino, M.; Chirone, R.; Lisi, L.; Pirone, R.; Salatino, P.; Russo, G. Cu/ $\gamma$ -Al<sub>2</sub>O<sub>3</sub> catalyst for the combustion of methane in a fluidized bed reactor. *Catal. Today* **2002**, *75*, 317–324. [[CrossRef](#)]
5. Foka, M.; Chaouki, J.; Guy, C.; Klvana, D. Natural gas combustion in a catalytic turbulent fluidized bed. *Chem. Eng. Sci.* **1994**, *49*, 4269–4276. [[CrossRef](#)]
6. Simonov, A.; Yazykov, N.; Vedyakin, P.; Lavrov, G.; Parmon, V. Industrial experience of heat supply by catalytic installations. *Catal. Today* **2000**, *60*, 139–145. [[CrossRef](#)]
7. Simonov, A.D.; Fedorov, N.A.; Dubinin, Y.V.; Yazykov, N.A.; Yakovlev, V.A.; Parmon, V.N. Catalytic heat-generating units for industrial heating. *Catal. Ind.* **2013**, *5*, 42–49. [[CrossRef](#)]
8. Ismagilov, Z.R.; Shkrabina, R.A.; Koryabkina, N.A. New technology for production of spherical alumina supports for fluidized bed combustion. *Catal. Today* **1999**, *47*, 51–71. [[CrossRef](#)]
9. Klvana, D.; Delval, J.; Kirchnerova, J.; Chaouki, J. Deactivation of fiber-supported La<sub>0.65</sub>Sr<sub>0.35</sub>Ni<sub>0.29</sub>Co<sub>0.69</sub>Fe<sub>0.02</sub>O<sub>3</sub> catalyst by mercaptan during combustion of methane or natural gas. *Appl. Catal. A Gen.* **1997**, *165*, 171–182. [[CrossRef](#)]
10. Mahato, N.; Banerjee, A.; Gupta, A.; Omar, S.; Balani, K. Progress in material selection for solid oxide fuel cell technology: A review. *Prog. Mater. Sci.* **2015**, *72*, 141–337. [[CrossRef](#)]
11. Rosso, I.; Garrone, E.; Geobaldo, F.; Onida, B.; Saracco, G.; Specchia, V. Sulphur poisoning of LaMn<sub>1-x</sub>Mg<sub>x</sub>O<sub>3</sub> catalysts for natural gas combustion. *Appl. Catal. B Environ.* **2001**, *30*, 61–73. [[CrossRef](#)]
12. Buelna, G.; Lin, Y.S. Sol-gel-derived mesoporous  $\gamma$ -alumina granules. *Microporous Mesoporous Mater.* **1999**, *30*, 359–369. [[CrossRef](#)]

13. Islam, A.; Taufiq-Yap, Y.H.; Chu, C.-M.; Chan, E.-S.; Ravindra, P. Synthesis and characterization of millimetric gamma alumina spherical particles by oil drop granulation method. *J. Porous Mater.* **2012**, *19*, 807–817. [[CrossRef](#)]
14. Shepeleva, M.N.; Shkrabina, R.A.; Ismagilov, Z.R.; Fenelonov, V.B. Preparation of Strong Alumina Supports for Fluidized Bed Catalysts. *Stud. Surf. Sci. Catal.* **1991**, *63*, 583–590.
15. Arendarskii, D.A.; Ismagilov, Z.R.; Barannik, G.B. Study of the deactivation and regeneration of copper chromite on  $\gamma$ -alumina and magnesium chromite on  $\gamma$ -alumina catalysts for fuel combustion. *Catal. Lett.* **1992**, *15*, 347–351. [[CrossRef](#)]
16. Shanker, A.K.; Cervantes, C.; Loza-Tavera, H.; Avudainayagam, S. Chromium toxicity in plants. *Environ. Int.* **2005**, *31*, 739–753. [[CrossRef](#)]
17. Miki, T.; Tai, Y. Catalytic Oxidation of Toluene over  $\text{Fe}_2\text{O}_3/\text{Al}_2\text{O}_3$  Catalyst. *Mater. Sci. Forum* **2011**, *695*, 101–104. [[CrossRef](#)]
18. Abdel Halim, K.S.; Khedr, M.H.; Nasr, M.I.; El-Mansy, A.M. Factors affecting CO oxidation over nanosized  $\text{Fe}_2\text{O}_3$ . *Mater. Res. Bull.* **2007**, *42*, 731–741. [[CrossRef](#)]
19. Liu, X.; Liu, J.; Chang, Z.; Sun, X.; Li, Y. Crystal plane effect of  $\text{Fe}_2\text{O}_3$  with various morphologies on CO catalytic oxidation. *Catal. Commun.* **2011**, *12*, 530–534. [[CrossRef](#)]
20. Fedorov, A.V.; Tsapina, A.M.; Bulavchenko, O.A.; Saraev, A.A.; Odegova, G.V.; Ermakov, D.Y.; Zubavichus, Y.V.; Yakovlev, V.A.; Kaichev, V.V. Structure and Chemistry of Cu–Fe–Al Nanocomposite Catalysts for CO Oxidation. *Catal. Lett.* **2018**, *148*, 3715–3722. [[CrossRef](#)]
21. Cheng, T.; Fang, Z.; Hu, Q.; Han, K.; Yang, X.; Zhang, Y. Low-temperature CO oxidation over  $\text{CuO}/\text{Fe}_2\text{O}_3$  catalysts. *Catal. Commun.* **2007**, *8*, 1167–1171. [[CrossRef](#)]
22. Cao, J.-L.; Wang, Y.; Yu, X.-L.; Wang, S.-R.; Wu, S.-H.; Yuan, Z.-Y. Mesoporous  $\text{CuO}-\text{Fe}_2\text{O}_3$  composite catalysts for low-temperature carbon monoxide oxidation. *Appl. Catal. B* **2008**, *79*, 26–34. [[CrossRef](#)]
23. Litt, G.; Almquist, C. An investigation of  $\text{CuO}/\text{Fe}_2\text{O}_3$  catalysts for the gas-phase oxidation of ethanol. *Appl. Catal. B* **2009**, *90*, 10–17. [[CrossRef](#)]
24. Bulavchenko, O.A.; Vinokurov, Z.S.; Saraev, A.A.; Tsapina, A.M.; Trigub, A.L.; Gerasimov, E.Y.; Gladky, A.Y.; Fedorov, A.V.; Yakovlev, V.A.; Kaichev, V.V. The Influence of Cu and Al Additives on Reduction of Iron(III) Oxide: In Situ XRD and XANES Study. *Inorg. Chem.* **2019**, *58*, 4842–4850. [[CrossRef](#)] [[PubMed](#)]
25. Saraev, A.A.; Tsapina, A.M.; Fedorov, A.V.; Trigub, A.L.; Bulavchenko, O.A.; Vinokurov, Z.S.; Zubavichus, Y.V.; Kaichev, V.V. CuFeAl-composite catalysts of oxidation of gasification products of solid fuels: In situ XAS and XRD study. *Radiat. Phys. Chem.* **2020**, in press. [[CrossRef](#)]
26. Hiramatsu, Y.; Oka, Y. Determination of the tensile strength of rock by a compression test of an irregular test piece. *Int. J. Rock Mech. Min. Sci. Geomech. Abstr.* **1966**, *3*, 89–90. [[CrossRef](#)]
27. ASTM D4179-11. *Standard Test Method for Single Pellet Crush Strength of Formed Catalysts and Catalyst Carriers*; ASTM International: West Conshohocken, PA, USA, 2017.
28. Wu, D.; Zhou, J.; Li, Y. Mechanical strength of solid catalysts: Recent developments and future prospects. *AIChE J.* **2007**, *53*, 2618–2629. [[CrossRef](#)]
29. Zakeri, M.; Samimi, A.; Afarani, M.S.; Salehirad, A. Interaction between Weibull parameters and mechanical strength reliability of industrial-scale water gas shift catalysts. *Particuology* **2017**, *32*, 160–166. [[CrossRef](#)]
30. Wu, D.; Li, Y.; Shi, Y.; Fang, Z.; Wu, D.; Chang, L. Effects of the calcination conditions on the mechanical properties of a  $\text{PCoMo}/\text{Al}_2\text{O}_3$  hydrotreating catalyst. *Chem. Eng. Sci.* **2002**, *57*, 3495–3504. [[CrossRef](#)]
31. Fedorov, A.V.; Gulyaeva, Y.K. Strength statistics for porous alumina. *Powder Technol.* **2019**, *343*, 783–791. [[CrossRef](#)]
32. Antonyuk, S.; Tomas, J.; Heinrich, S.; Mörl, L. Breakage behaviour of spherical granulates by compression. *Chem. Eng. Sci.* **2005**, *60*, 4031–4044. [[CrossRef](#)]
33. Cimino, S.; Pirone, R.; Russo, G. Thermal Stability of Perovskite-Based Monolithic Reactors in the Catalytic Combustion of Methane. *Ind. Eng. Chem. Res.* **2001**, *40*, 80–85. [[CrossRef](#)]
34. Arai, H.; Machida, M. Thermal stabilization of catalyst supports and their application to high-temperature catalytic combustion. *Appl. Catal. A* **1996**, *138*, 161–176. [[CrossRef](#)]
35. Arai, H.; Fukuzawa, H. Research and development on high temperature catalytic combustion. *Catal. Today* **1995**, *26*, 217–221. [[CrossRef](#)]

36. Bulavchenko, O.A.; Pochtar', A.A.; Gerasimov, E.Y.; Fedorov, A.V.; Chesalov, Y.A.; Saraev, A.A.; Yakovlev, V.A.; Kaichev, V.V. Chemical and texture promoters in Cu-Fe-Al oxide nanocomposite catalysts for combustion of solid fuel gasification products. *Appl. Catal. A* **2020**, *590*, 117364. [[CrossRef](#)]
37. Luo, M.-F.; Fang, P.; He, M.; Xie, Y.-L. In situ XRD, Raman, and TPR studies of CuO/Al<sub>2</sub>O<sub>3</sub> catalysts for CO oxidation. *J. Mol. Catal. A* **2005**, *239*, 243–248. [[CrossRef](#)]
38. He, M.; Luo, M.; Fang, P. Characterization of CuO Species and Thermal Solid-Solid Interaction in CuO/CeO<sub>2</sub>-Al<sub>2</sub>O<sub>3</sub> Catalyst by In-Situ XRD, Raman Spectroscopy and TPR. *J. Rare Earths* **2006**, *24*, 188–192. [[CrossRef](#)]
39. Zieliński, J.; Zglinicka, I.; Znak, L.; Kaszkur, Z. Reduction of Fe<sub>2</sub>O<sub>3</sub> with hydrogen. *Appl. Catal. A Gen.* **2010**, *381*, 191–196. [[CrossRef](#)]
40. Wang, H.; Zhang, Q.; Zhang, T.; Wang, J.; Wei, G.; Liu, M.; Ning, P. Structural tuning and NH<sub>3</sub>-SCO performance optimization of CuO-Fe<sub>2</sub>O<sub>3</sub> catalysts by impact of thermal treatment. *Appl. Surf. Sci.* **2019**, *485*, 81–91. [[CrossRef](#)]
41. Basu, P. Combustion of coal in circulating fluidized-bed boilers: A review. *Chem. Eng. Sci.* **1999**, *54*, 5547–5557. [[CrossRef](#)]
42. Ismagilov, Z.R.; Kerzhentsev, M.A.; Besidin, V.I.; Susharina, T.L. Formation of nitrogen oxides in the oxidation of pyridine on some oxide catalysts. *React. Kinet. Catal. Lett.* **1983**, *23*, 49–54. [[CrossRef](#)]
43. Ismagilov, Z.R.; Kerzhentsev, M.A. Catalytic Fuel Combustion—A Way of Reducing Emission of Nitrogen Oxides. *Catal. Rev.* **1990**, *32*, 51–103. [[CrossRef](#)]
44. Ni, W.; Li, H.; Zhang, Y.; Zou, Z. Effects of Fuel Type and Operation Parameters on Combustion and NO<sub>x</sub> Emission of the Iron Ore Sintering Process. *Energies* **2019**, *12*, 213. [[CrossRef](#)]



© 2020 by the authors. Licensee MDPI, Basel, Switzerland. This article is an open access article distributed under the terms and conditions of the Creative Commons Attribution (CC BY) license (<http://creativecommons.org/licenses/by/4.0/>).